J. Fluid Mech. (2003), *vol.* 478, *pp.* 11–34.
DOI: 10.1017/S0022112002003324 Printed in the United Kingdom

Turbulence over a compliant surface: numerical simulation and analysis

By S. XU[1], D. REMPFER[2] AND J. LUMLEY[1]

[1]Sibley School of Mechanical and Aerospace Engineering, Cornell University, Ithaca, NY 14853, USA
[2]Department of Mechanical, Materials and Aerospace Engineering, Illinois Institute of Technology, Chicago, IL 60616, USA

(Received 26 July 2002 and in revised form 8 October 2002)

In this paper we present results from a numerical investigation of turbulent channel flow in the presence of a compliant wall. The compliant wall is modelled as a homogeneous spring-supported plate. The simulation code is validated both by comparison with an alternative code and by reproducing results of linear stability theory. Our results demonstrate that with the wall compliance we used in the simulation there is little change in the very long-time behaviour of the turbulent skin friction drag and little modification to the near-wall turbulent coherent structures. The values of pertinent statistical quantities of the turbulence near the compliant walls converge to those near a rigid wall and the statistical effect of the wall compliance on the turbulent channel flow is small.

1. Introduction

The flow in and around many technical devices creates turbulent boundary layers, which can lead to significant losses in efficiency. Thus, reducing this turbulent drag, which is responsible for a large part of the drag experienced by airplanes, ships and submarines, and reducing turbulent sound production, which, among other things, is the major source responsible for the noise inside the cabin of transport aircraft, are particularly desirable goals. Skin friction reduction can be achieved through various methods of boundary layer manipulation, which include active or passive transition delay and turbulence control. A number of strategies have been proposed for this purpose, such as polymer or particle additives, blowing and suction, LEBUs, riblets, and compliant coatings, as well as methods for active control. Reactive boundary layer manipulation requires sensors, actuators and control algorithms. The necessary technology is far from mature at present and it is not clear whether the associated development effort will ultimately pay off (Lumley & Blossey 1998). The use of compliant walls as a simpler passive means appears an attractive alternative (Gad-el-Hak 1998) . In particular, although the maximum amount of drag reduction that can be achieved using compliant walls may be less than that demonstrated numerically for methods of reactive turbulence control, compliant walls do not use any energy to achieve their drag-reducing effect. This is in stark contrast to methods for reactive turbulence control, which usually require significant amounts of energy, which, in all experiments that have been done up to now, far exceed the energy that could be saved via drag reduction.

Thus the idea of using a compliant wall with a tailored dynamic response to pressure disturbances from a turbulent wall layer is a potentially attractive one. Having said

that, we are well aware of the history of related research some twenty-five years ago. At that time, following observations by Kramer (1961) on exceptional swimming capabilities of dolphins, there was a long series of what now has to be described as failed experimental attempts to verify compliant wall technology. This body of work is described in Bushnell, Hefner & Ash (1977). After these negative results, studies of this type were effectively discredited, at least from an experimental point of view. With regard to this history, two more points are worth noting:

(i) The exact reasons for the failure of the experiments were not always clear, and, in particular, to this day nothing definitive can be said about whether or not compliant surfaces may be able to significantly reduce turbulent drag or sound production. We believe that the obvious benefits that compliant surfaces may give warrant taking another, more detailed look at this problem, in our case from a more theoretical perspective and using modern approaches based on low-dimensional modelling (Rempfer *et al.* 2001), and direct numerical simulations of turbulent flows.

(ii) Despite the relative wealth of experimental data, there are very few results available on the effect of compliant walls on the structure and properties of *turbulent* wall layers. Kireiko (1991) analysed the interaction of a compliant wall with near-wall turbulence by using the monoharmonic approximation and concluded that the interaction appears resonant in character and a considerable reduction in turbulent skin friction may be possible for certain values of wall parameters. Semenov (1991) proposed a set of conditions for modelling and choosing viscoelastic coatings for drag reduction according to a hydraulic smoothness requirement and interference theory, in which the linear harmonic solution to the interaction is obtained for a given pressure fluctuation spectrum using a simplified linear near-wall turbulence model. The first of his conditions is a requirement of quick attenuation or absence of free vibrations of the coating. The second one requires a limitation of the coating compliance such that the allowable amplitude of the wall deformation remains below $r^+ = 6$ (where r^+ is the wall roughness height in wall units). The third condition states that the natural frequency of the wall should be chosen in order to ensure a large phase–frequency region of favourable interaction. Kang & Choi (2000) have studied active walls deformed according to successful control strategies for drag reduction in turbulent channel flows. They found that overall 13%—17% drag reduction can be obtained with active wall motions. Turbulence intensity and near-wall streamwise vortices can be significantly weakened and instantaneous wall shapes are elongated in the streamwise direction. From these results it is natural to ask whether it might be possible to design a compliant surface with elastic properties such that the wall, driven by pressure disturbances from the flow, would move 'by itself' in the same way as the one used in Kang & Choi's study. It is this question that we will study in more detail below.

We also note that a number of investigations have been aimed at delaying boundary layer transition (which is a relevant flow regime in the case of the dolphin) using compliant coatings. Results of numerical studies indicating benefits from compliant walls in the area of transition delay were reported by Carpenter & Morris (1990) and by Davies & Carpenter (1997). The case of transition manipulation is interesting, because in that case there is quite an extensive body of theoretical material on this problem, which is described by the linear stability theory and the asymptotic theory of transitional flows over compliant walls or in compliant channels (see Gajjar & Sibanda 1996; Larose & Grotberg 1996; Lucey & Carpenter 1995; Reutov & Rybushkina 1998; Riley, Gad-el-Hak & Metcalfe 1988; Yeo, Khoo & Zhao 1999). In fact, linear stability theory can provide satisfactory explanations for the failure of

many experimental attempts aimed at delaying the onset of transition over compliant walls. It turns out that substantial postponement of laminar–turbulent transition is possible through the use of properly designed compliant walls and laminar flow may be maintained to indefinitely high Reynolds numbers through the use of multiple-panel compliant walls tailored for the local flow environment (Carpenter, Davies & Lucey 2000).

In the present paper we investigate the interaction of a compliant wall with turbulence by performing direct numerical simulations of a turbulent flow in a minimal channel flow unit (MFU) (Jiménez & Moin 1991). The MFU represents a channel flow with periodic boundary conditions for the spanwise coordinate. The fundamental spanwise wavelength of the MFU represents the smallest width of such a channel at which sustained turbulence is possible. Physically this means that, on average, the MFU can accommodate just one pair of the vitally important high- and low-speed streaks and corresponding rolls of near-wall turbulence. The advantage of this setup is that it allows us to perform direct numerical simulations with a minimal amount of computational effort. Since we have found that one needs to simulate the flow dynamics over times spanning several thousand outer units in order to achieve reliable statistics (see below), this simplification was vital at the current exploratory stage of our work. It is also worth mentioning that the MFU, despite this simplification, still retains all of the fundamental physics of turbulence, see Jiménez & Moin (1991).

Two questions arise regarding this investigation. What phenomena are observed? What are the mechanisms behind these phenomena (and how can we possibly exploit these mechanisms in order to minimize turbulent drag)? Since we are reporting work in progress here, we mainly describe our preliminary answers to the first question.

2. Fundamental equations

The problem we are considering is basically a fluid–solid problem. On the fluid side, we have the incompressible Navier–Stokes equations as the model for fluid motion. On the solid side, we use a spring-supported plate to model a compliant wall. The equation governing the wall-normal motion of this plate non-dimensionalized by the average half-channel height h and the laminar centerline velocity u_0 reads

$$C_0\frac{\partial^2\eta}{\partial t^2}+C_1\frac{\partial\eta}{\partial t}+C_2\left(\frac{\partial^4\eta}{\partial x_1^4}+\frac{\partial^4\eta}{\partial x_3^4}+2\frac{\partial^4\eta}{\partial x_1^2x_3^2}\right)+C_3\eta-C_x\frac{\partial^2\eta}{\partial x_1^2}-C_z\frac{\partial^2\eta}{\partial x_3^2}=-p_w, \quad (2.1)$$

where η is the wall-normal displacement, p_w is the pressure disturbance on the wall and C_0, C_1, C_2, C_3, and $C_x(C_z)$ are the non-dimensional wall properties defined as

$$\left.\begin{aligned} C_0=\frac{\rho_m b}{\rho h}, \quad C_1=\frac{1}{Re}\frac{dh}{\rho\nu}, \quad C_2=\frac{1}{Re^2}\frac{B}{\rho h\nu^2},\\ C_3=\frac{1}{Re^2}\frac{K_E h^3}{\rho\nu^2}, \quad C_x=\frac{1}{Re^2}\frac{T_x h}{\rho\nu^2}, \quad C_z=\frac{1}{Re^2}\frac{T_z h}{\rho\nu^2}. \end{aligned}\right\} \quad (2.2)$$

The wall parameters are: the plate density ρ_m and thickness b, the wall damping coefficient d, the flexural rigidity of the plate B, the streamwise (spanwise) tension per unit width $T_x(T_z)$ and the spring stiffness K_E; ρ is the density of the fluid and ν is its kinematic viscosity. We will assume that our wall is homogeneous, with uniform elastic properties, so that all of the above parameters are constant except the damping coefficient.

Depending on our choice of parameters, the compliant wall can act like a thin membrane (for $B \to 0$), or like a rigid plate (when $B \to \infty$). For the cases to be

discussed below, we have chosen walls that are very flexible, closely approximating the behaviour of a thin membrane. The turbulent channel flow we simulate is assumed periodic in the streamwise (x_1 or x) and spanwise (x_3 or z) directions and has a rigid upper wall and a compliant lower wall that are separated by an average distance of $2h$ in the wall-normal (x_2 or y) direction. Re is its Reynolds number based on h and u_0.

The main difficulty of the simulation is handling the boundary conditions at the moving compliant wall. We use a time-varying coordinate transformation to eliminate the deformation of the compliant boundary in the computational domain. The continuity equation in the computational coordinate system becomes

$$u^i_{;i} = 0, \tag{2.3}$$

and the momentum equation in the rotational form becomes

$$\frac{\partial u^i}{\partial t} = -\frac{\partial T^{-1}}{\partial t}\frac{\partial u^i}{\partial x_2} + u^j g^{ik}(u_{j;k} - u_{k;j}) - g^{ij}\frac{\partial p}{\partial x_j} + \frac{1}{Re}\left(g^{jk}u^i_{;k}\right)_{;j}, \tag{2.4}$$

where u^i is a contravariant velocity component, the semicolon denotes covariant differentiation, T^{-1} is the inverse coordinate transformation function in the wall-normal direction, and g^{ij} is the contravariant metric tensor of the transformation. The equation for pressure p is obtained by taking a covariant differentiation with respect to x_i of the momentum equation (2.4) and can be written as

$$\left(g^{ij}\frac{\partial p}{\partial x_j}\right)_{;i} = \left[-\frac{\partial T^{-1}}{\partial t}\frac{\partial u^i}{\partial x_2} + u^j g^{ik}(u_{j;k} - u_{k;j})\right]_{;i}. \tag{2.5}$$

The boundary conditions for velocity must also be transformed into the new coordinate system. The boundary conditions for pressure can then be determined indirectly from the incompressibility condition via an influence matrix technique. A Fourier–Galerkin and Chebyshev–Tau pseudospectral method for spatial discretization and a three-sub-step Runge–Kutta method for time advancement are used for solving the equations. For detailed numerical procedures we refer to Carlson, Berkooz & Lumley (1995).

3. Results

The computational domain sizes in the streamwise and spanwise directions are $L_x = L_z = 4\pi/5$ and the computation is carried out using $32 \times 65 \times 96$ (in x, y, z) grid points for a Reynolds number of 3000. We are simulating the evolution of the flow in a three-dimensional channel that has a compliant wall at $y = -1$ and a rigid wall at $y = 1$. In addition, as a reference case for comparisons, we have simulated the turbulent flow in a canonical channel composed of two rigid walls with the same flow parameters as those for the compliant-wall cases. In each case the mean pressure gradient is calculated at each time step to enforce constant mass flux in the channel. We have checked that increasing our grid resolution does not significantly change the results. Also, the energy spectra indicate that the resolution of the simulation is sufficient.

3.1. *Code validation*

The reliability of the simulation depends on whether the code can accurately represent the velocity boundary conditions on a moving boundary, which can be tested using active (prescribed) wall motion. If the wall deformation amplitude is

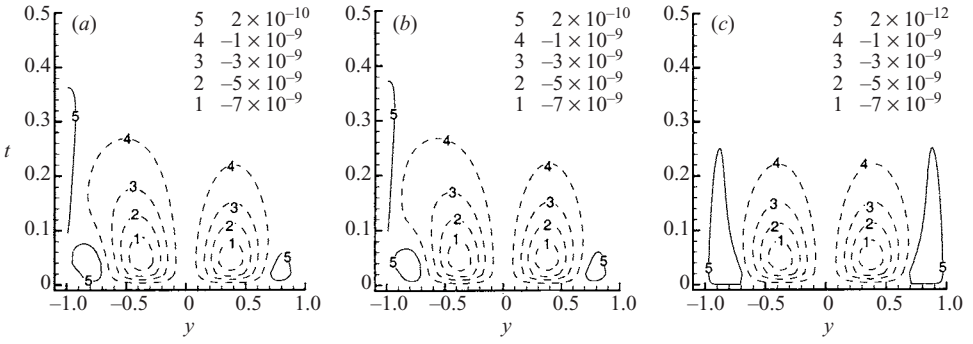

FIGURE 1. Time evolution of the production term $-\langle uv\rangle \mathrm{d}u/\mathrm{d}y$ for channel flows at $Re = 3$ with identical initial conditions. (*a*) Flow simulated using linearized boundary conditions in a channel having one compliant wall with average position at $y = -1$. (*b*) Flow in the same channel simulated by the direct simulation code using coordinate transformation. (*c*) Flow in a canonical rigid channel.

large enough, nonlinearity will set in. These nonlinear tests have been performed, successfully, by Carlson *et al.* (1995).

In order to further validate our code and confirm that we can achieve a numerical accuracy that is appropriate for the effects we are interested in, we have performed two additional types of assessments. The first of these compares the results obtained with two different nonlinear DNS codes, which differ in the way the boundary conditions are implemented, as described in the following paragraph. As a second test, we used our DNS codes to simulate the behaviour of very small disturbances and checked that the DNS solutions reproduce results from linear stability theory.

3.1.1. *Linear tests*

When the displacement of the compliant wall is very small, the velocity boundary conditions at the moving wall can be linearized. We developed a code using such linearized boundary conditions to simulate a laminar flow with parabolic mean and two-dimensional disturbances in a compliant channel. We emphasize that linearized boundary conditions were used for the sole purpose of validating the accuracy of our code using coordinate transformation, which is equivalent to a fully general, nonlinear boundary condition. All of the results presented in § 3.3 of this paper were obtained with the general nonlinear boundary conditions. As shown in figures 1–3, the flow evolution and the compliant-wall motion agree well with those simulated by our direct simulation code using a time-dependent coordinate transformation. Thus, we can assume that this coordinate transformation correctly captures the effects of the moving compliant wall in our simulation.

3.1.2. *Comparison with linear theory*

In addition, in order to assess the accuracy with which our numerical scheme couples the compliant wall motion with the fluid dynamics of the flow and integrates the transport of momentum as described by the Navier–Stokes equation, we can also test our codes by comparing the temporal growth rates computed from direct simulation with those from the linear stability theory for small-amplitude disturbances in a compliant channel.

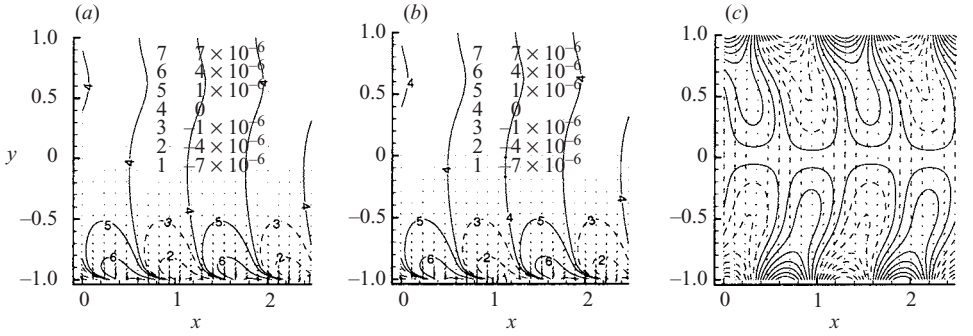

FIGURE 2. Velocity and pressure field at time $t = 2$ for the same flows as in figure 1(a–c).

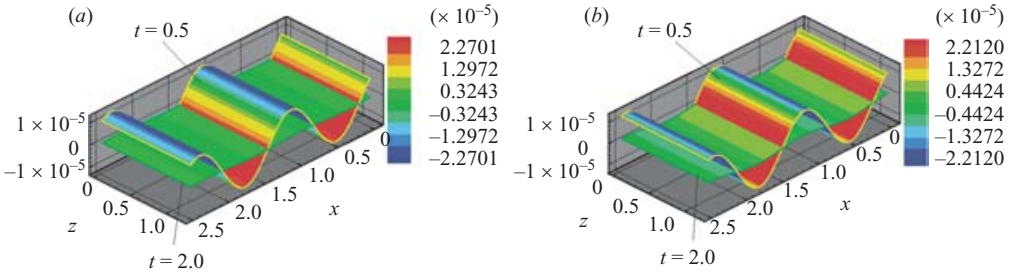

FIGURE 3. Displacement and contours of the wall-normal velocity at two different times at the compliant wall of the channel. (a) Simulation using linearized boundary conditions. (b) Simulation using coordinate transformation.

For the purposes of this test it is sufficient to consider two-dimensional disturbances only. The disturbance streamfunction for this case is

$$\Psi(x, y, t) = \phi(y)\mathrm{e}^{\mathrm{i}\alpha(x-ct)}, \tag{3.1}$$

where α is the wavenumber and $c = c_r + c_i\mathrm{i}$ is the phase velocity. Substituting Ψ into the linearized vorticity equation gives the Orr–Sommerfeld equation,

$$(U - c)(\mathrm{D}^2 - \alpha^2)\phi - \mathrm{D}^2 U\phi = \frac{1}{\mathrm{i}\alpha Re}(\mathrm{D}^2 - \alpha^2)^2\phi, \tag{3.2}$$

where $U(y) = 1 - y^2$ is the mean velocity profile and $\mathrm{D} := \mathrm{d}/\mathrm{d}y$. The pressure disturbance and the compliant wall displacement can be written as

$$p(x, y, t) = \hat{p}(y)\mathrm{e}^{\mathrm{i}\alpha(x-ct)}, \quad \eta(x, t) = \hat{\eta}\mathrm{e}^{\mathrm{i}\alpha(x-ct)}. \tag{3.3}$$

We assume that the effect of mean flow pressure gradient on the compliant wall is balanced in such a way that the average location of the wall is at $y = -1$. We define the wall admittance $Y(\alpha, c)$ as

$$Y(\alpha, c) = \frac{\mathrm{i}\alpha c}{\alpha^2 c^2 C_0 + \mathrm{i}C_1\alpha c - (\alpha^4 C_2 + \alpha^2 C_x + C_3)}, \tag{3.4}$$

which gives the ratio of the wall velocity to the perturbation fluid pressure at the wall. Thus we have

$$\hat{p}(-1) = \frac{\mathrm{i}\alpha c\hat{\eta}}{Y(\alpha, c)}. \tag{3.5}$$

From the x-momentum equation for the fluid we can obtain the disturbance pressure on the wall as

$$\hat{p}(-1) = \left\{ \left[-(U-c) + \frac{1}{\mathrm{i}\alpha Re}(\mathrm{D}^2 - \alpha^2) \right] \mathrm{D}\phi + \mathrm{D}U\phi \right\}_{y=-1}. \tag{3.6}$$

No-slip and no-penetration boundary conditions on the upper rigid wall at $y = +1$ give

$$\mathrm{D}\phi(+1) = \phi(+1) = 0, \tag{3.7}$$

and the linearized boundary conditions at $y = -1$ are

$$\left.\begin{aligned} u(-1) \approx -\eta \mathrm{D}U(-1) &\Longrightarrow \mathrm{D}\phi(-1) = -\hat{\eta}\mathrm{D}U(-1), \\ v(-1) \approx \tfrac{\partial \eta}{\partial t} &\Longrightarrow \phi(-1) = c\hat{\eta}. \end{aligned}\right\} \tag{3.8}$$

If we eliminate $\hat{\eta}$, the boundary conditions (3.8) together with equation (3.6) can be written as

$$\left.\begin{aligned} \mathrm{D}U(-1)\phi(-1) + c\mathrm{D}\phi(-1) = 0, \\ \alpha\phi(-1) + \mathrm{i}Y(\alpha, c)\hat{p}(-1) = 0. \end{aligned}\right\} \tag{3.9}$$

We use a Chebyshev method (Zebib 1984) to solve the Orr–Somerfeld equation. After expanding $\phi^{(4)}$ in Chebyshev polynomials,

$$\phi^{(4)} = \sum_{j=0}^{N} a_j T_j, \tag{3.10}$$

and integrating (3.10) four times, we obtain

$$\left.\begin{aligned} \phi^{(3)} &= \sum_{j=0}^{N+1} \left(\sum_{i=0}^{N} f_{ji}^{(3)} a_j \right) T_j + c_1 T_0, \\ \phi^{(2)} &= \sum_{j=0}^{N+2} \left(\sum_{i=0}^{N} f_{ji}^{(2)} a_j \right) T_j + c_1 T_1 + c_2 T_0, \\ \phi^{(1)} &= \sum_{j=0}^{N+3} \left(\sum_{i=0}^{N} f_{ji}^{(1)} a_j \right) T_j + \frac{c_1}{4} T_2 + c_2 T_1 + c_3 T_0, \\ \phi &= \sum_{j=0}^{N+4} \left(\sum_{i=0}^{N} f_{ji}^{(0)} a_j \right) T_j + \frac{c_1}{24} T_3 + \frac{c_2}{4} T_2 + \left(c_3 - \frac{c_1}{8} \right) T_1 + c_4 T_0, \end{aligned}\right\} \tag{3.11}$$

where c_1, c_2, c_3 and c_4 are four integral constants. From the boundary conditions (3.7), (3.9), these four constants can be computed as

$$c_i = \sum_{j=0}^{N} c_{ij} a_j, \quad i = 1, 2, 3, 4. \tag{3.12}$$

In the above expression, c_{ij} takes the form

$$c_{ij} = \frac{N_{ij}(c)}{D_{ij}(c)}, \tag{3.13}$$

where the numerator and denominator are third-order polynomials with respect to the phase velocity c. The usual Galerkin procedure for the Orr–Sommerfeld equation (3.2)

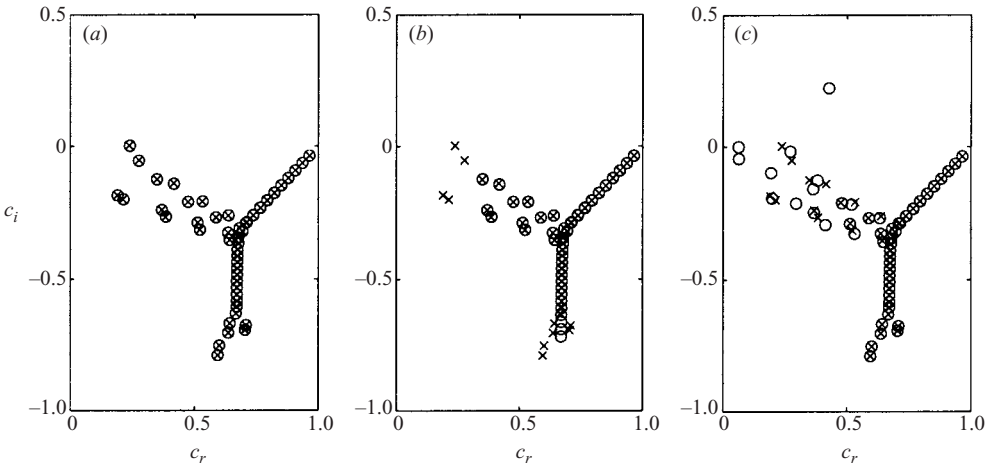

FIGURE 4. Comparison of eigenvalue ($c = c_r + c_i$i) spectra for two-dimensional flows with $Re = 10\,000$ and $\alpha = 1.0$ in compliant channels and a rigid channel. (*a*) The compliant channel has one compliant wall with $C_0 = 1$, $C_1 = 0$, $C_2 = 1 \times 10^{-6}$, $C_3 = 2$, $C_x = 2$. (*b*) The compliant channel has one compliant wall with $C_0 = 1$, $C_1 = 0$, $C_2 = 1 \times 10^{-6}$, $C_3 = 1$, $C_x = 1$. (*c*) The compliant channel has one compliant wall with $C_0 = 1$, $C_1 = 0$, $C_2 = 1 \times 10^{-6}$, $C_3 = 0.002$, $C_x = 0.002$. Crosses: rigid channel, circles: compliant channel.

then leads to a polynomial eigenvalue problem of the form

$$\left(\sum_{k=0}^{4} c^k L_k\right) a = 0, \tag{3.14}$$

where $a = (a_0, \ldots, a_N)$ is the vector formed by the Chebyshev coefficients and matrices L_k are independent of c. The companion matrix method (Bridges & Morris 1984) is used to solve the problem.

Our linear stability analysis indicates that compliance of one wall of a plane channel can modify or eliminate eigenmodes that are found in the corresponding rigid channel and also bring new eigenmodes. With increasing wall compliance, we observe how the unique unstable eigenmode present in the rigid channel is first slightly modified (figure 4*a*), before being eliminated completely (figure 4*b*). If we make the wall still 'softer', new unstable eigenmodes appear (figure 4*c*).

Due to the use of a time-dependent coordinate transformation in our direct simulation, the computational mesh for a compliant channel is varying in time. In order to validate this code, we therefore picked the unstable eigenmode for a rigid channel as given in figure 5(*a*) for our first test, and computed its growth rate as obtained from the data of a direct simulation to compare it with that from the linear theory. Thus, for this test the motion of the compliant wall is 'turned off', turning the compliant channel into a rigid one. The complex phase velocity computed from the direct simulation code is $c_S = 0.237526 + 0.00373967$i, which perfectly matches the eigenvalue $c_l = 0.237526 + 0.00373967$i from linear theory.

In order to be able to perform a comparison with linear theory for the case of a compliant wall, we picked the eigenmode given in figure 5(*b*). Since the moving mesh makes it difficult to directly compare results from linear theory to data from the DNS code that uses exact boundary conditions, we use the DNS with linearized boundary conditions for this second comparison. Thus, we compare the complex phase velocity

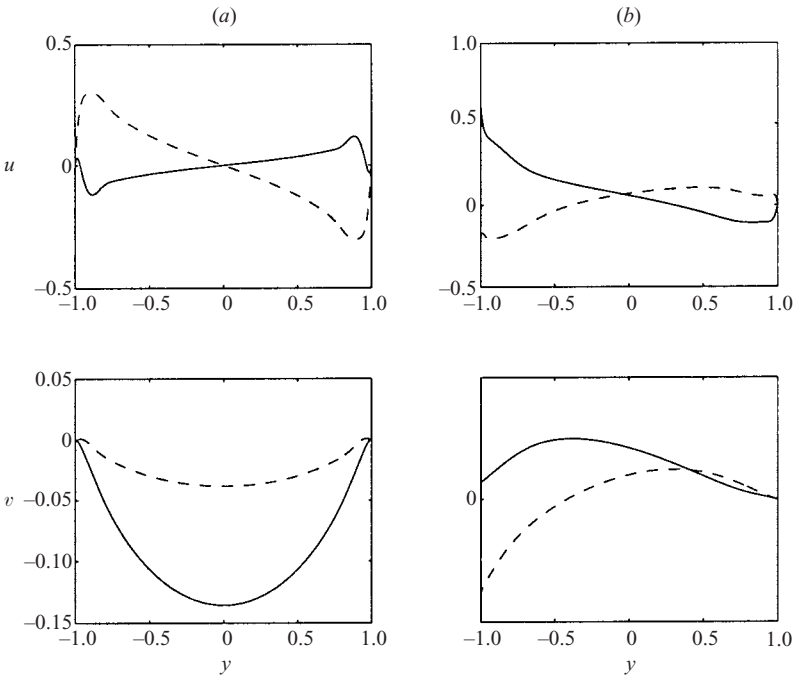

FIGURE 5. Normalized eigenfunctions for the u- and v-component of the disturbance velocity, for two-dimensional flow with $Re = 10,000$ and $\alpha = 1.0$ in (a) a canonical rigid channel with the corresponding phase velocity $c = 0.237526 + 0.00373967\mathrm{i}$, and ($b$) a compliant channel having one compliant wall with $C_0 = 1$, $C_1 = 0$, $C_2 = 1 \times 10^{-6}$, $C_3 = 0.002$, $C_x = 0.002$ and the corresponding phase velocity $c = 0.427352 + 0.221993\mathrm{i}$. Solid line: real part, dashed line: imaginary part.

of the eigenmode in figure 5(b), $c_l = 0.427352 + 0.221993\mathrm{i}$, to that obtained from our DNS code using linearized boundary conditions. The phase velocity obtained from the direct simulation for this case is $c_S = 0.427241 + 0.221097\mathrm{i}$, indicating excellent agreement. In addition, in figure 6 we are comparing the distribution of the disturbance amplitude along the y-coordinate as obtained from our DNS code to the corresponding linear eigenfunctions. Again, the two velocity distributions show very good agreement. Since we have also shown above that the two DNS codes produce results that closely match, we are confident that our coordinate transformation can accurately simulate the effect of a compliant wall in a turbulent channel.

3.2. *Monoharmonic analysis*

An important issue in this investigation of the interaction of turbulence with a compliant wall is the question of how to choose the values of the compliant wall parameters. There exists little theoretical guidance in this respect. A compliant wall should not be too compliant otherwise flutter, see figure 4(c), and static-divergence waves will appear and the skin friction will increase. We have seen a static wave on a compliant wall in our trial simulation, which grew with time and caused the simulation to diverge. The wave did not, however, take the peculiar shape revealed in the experiments of Gad-el-Hak, Blackwelder & Riley (1984). Lucey *et al.* (1997) have shown that it is necessary to include nonlinear effects in both the fluid and wall dynamics to explain the peculiar shape.

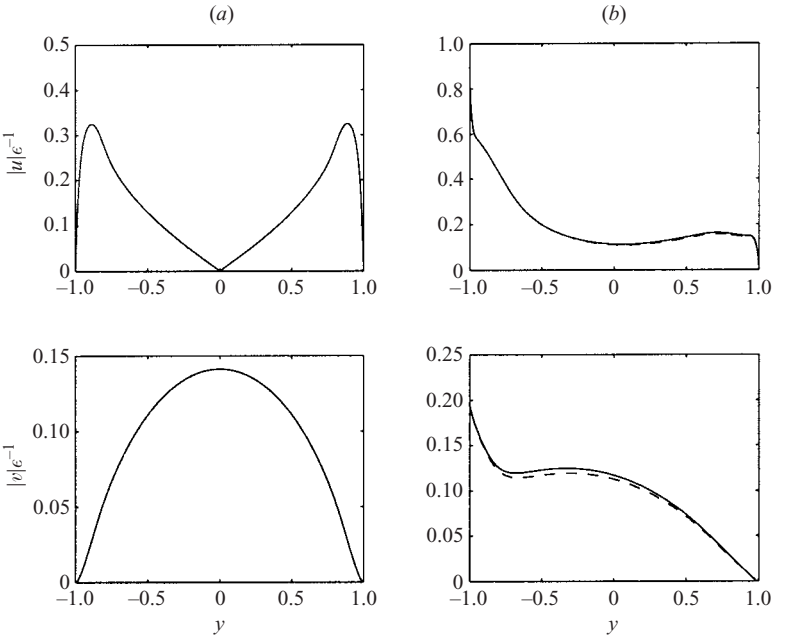

FIGURE 6. Amplitude of disturbance velocity u and v at time $t=1$ corresponding to (a) figure 5(a) and (b) figure 5(b). ϵ is a small positive constant used to initialize the amplitude of the disturbances in the direct simulation codes. Solid line: linear stability theory, dashed line: direct simulation.

The numerical requirements for the values of the compliant wall parameters are straightforward. A compliant wall should move intensively enough so that it physically interacts with turbulence rather than just generating some numerical noise in the computational system. The small time scales of wall motion associated with pressure disturbances of high wavenumbers have to be large enough to guarantee an acceptable time step in the numerical simulation. Monoharmonic analysis can give us a reference to choose a compliant wall to satisfy these numerical requirements.

In a monoharmonic approximation for compliant wall motion, a forcing pressure disturbance is given in a harmonic form:

$$p_w = \mathrm{Re}[\hat{p}_w \mathrm{e}^{\mathrm{i}k_x x + \mathrm{i}k_z z - \mathrm{i}\sigma t}]. \tag{3.15}$$

The natural circular frequency ω of the damped vibration and the time constant C_τ for damping of the compliant wall are then found to be

$$\omega = \begin{cases} 0 \quad (\text{no vibration}) & \text{if } \beta \geqslant 2\omega_n, \\ \frac{1}{2}\left|\beta^2 - 4\omega_n^2\right|^{1/2} & \text{if } \beta < 2\omega_n, \end{cases} \tag{3.16}$$

$$C_\tau = \begin{cases} 2\left[\beta - \left(\beta^2 - 4\omega_n^2\right)^{1/2}\right]^{-1} & \text{if } \beta \geqslant 2\omega_n, \\ 2\beta^{-1} & \text{if } \beta < 2\omega_n, \end{cases} \tag{3.17}$$

where β and ω_n are defined as

$$\beta = \frac{C_1}{C_0}, \quad \omega_n^2 = \frac{1}{C_0}\left[C_2\left(k_x^4 + k_z^4 + 2k_x^2 k_z^2\right) + C_x k_x^2 + C_z k_z^2 + C_3\right]. \tag{3.18}$$

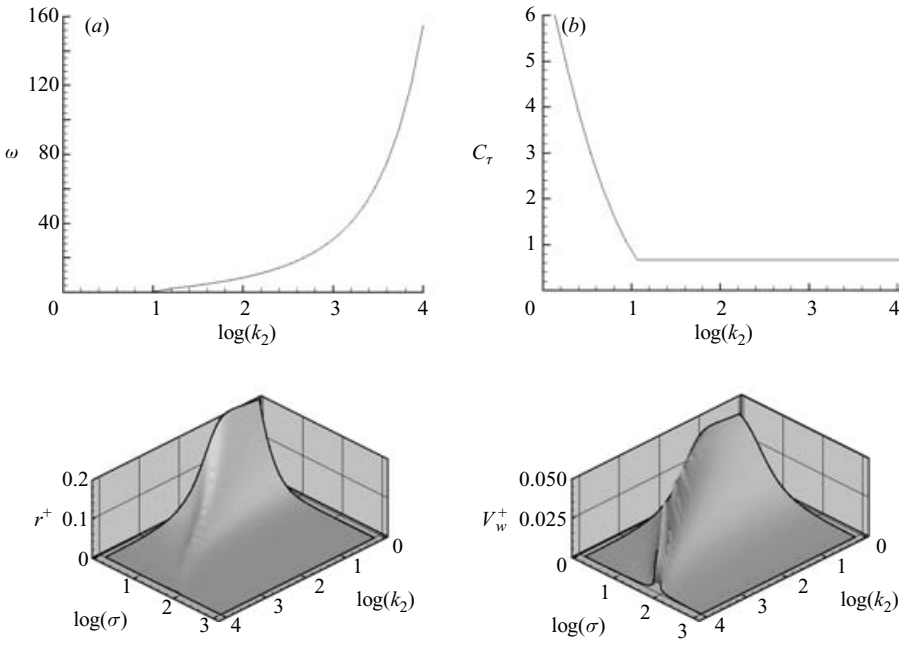

FIGURE 7. Results of the monoharmonic analysis for the motion of a compliant wall with $C_0 = 1$, $C_1 = 3$, $C_2 = 4 \times 10^{-5}$, $C_3 = 0.2$, $C_x = 0.2$, $C_z = 0.2$, $Re = 3000$, $Re_\tau = 137$, $\hat{p}_w = 0.01$. $k_2 = k_x^2 + k_z^2$.

The steady-state amplitude (in wall units) of the displacement r^+ and the wall-normal velocity V_w^+ of the compliant wall are

$$r^+ = \frac{K_d\, \hat{p}_w Re_\tau}{C_0 \omega_n^2}, \tag{3.19}$$

$$V_w^+ = \frac{K_d\, \hat{p}_w \sigma Re}{C_0 \omega_n^2 Re_\tau}. \tag{3.20}$$

Here, Re_τ is the turbulent Reynolds number on the compliant wall, and K_d is the dynamic coefficient which can be calculated from

$$K_d = \left[\left(1 - \frac{\sigma^2}{\omega_n^2} \right)^2 + \frac{\beta^2 \sigma^2}{\omega_n^4} \right]^{-1/2}. \tag{3.21}$$

Figure 7 shows the results of a monoharmonic analysis for the motion of a compliant wall that we used in the simulation. These and the later simulation results indicate that the compliant walls we used in the simulation satisfy the numerical requirements. The values of the compliant wall parameters in the simulation are given in table 1. Compliant wall II (Case II) has much smaller stretching than compliant wall I (Case I), but its spring stiffness is large to ensure stable wall–fluid interaction.

We mention that we have also tried other kinds of compliant walls. One of them has large flexural rigidity and tension. The very small time scales associated with its motion could not be captured by the simulation, ultimately leading to instability of the numerical simulation. We also tried a very soft wall, for which, as expected, the interaction with the flow is physically unstable. A static surface wave growing with

Parameters	Compliant Wall I	Compliant Wall II
C_0	1	0.8
C_1	$3\,(=2\zeta\omega_n C_0)$	$2\zeta\omega_n C_0$
C_2	4×10^{-5}	8×10^{-5}
C_3	0.2	0.8
C_x	0.2	0.008
C_z	0.2	0.008

TABLE 1. Values of the compliant wall parameters. $\zeta(=\beta/2\omega_n)$ is the damping ratio, as shown in figure 8.

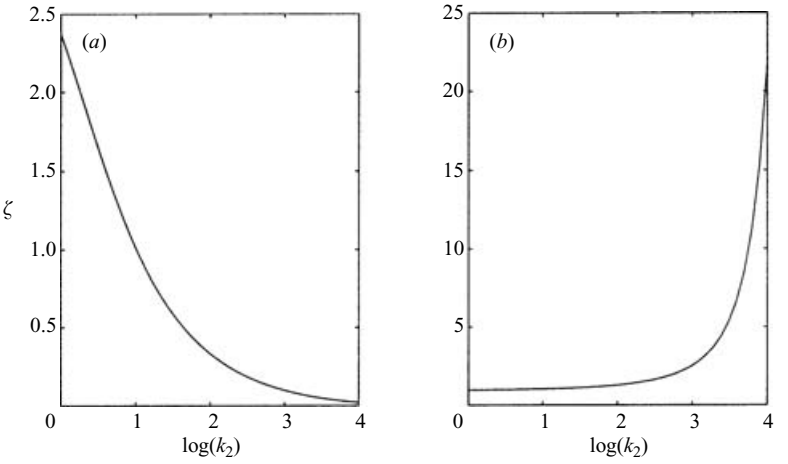

FIGURE 8. Damping ratio for (*a*) compliant wall I and (*b*) compliant wall II.

time in amplitude appeared which again leads to destabilization of the numerical code.

3.3. *Flow with wall compliance*

Figure 9 shows the history of the total drag (represented by the mean streamwise pressure gradient) and the skin friction coefficients for Case I and Case II against the reference case of a channel with two rigid walls. Because of the very small amplitude of the compliant wall displacement, the total drag is almost completely from the skin friction. Case II begins at time 1076, taking the flow field and the motion of the compliant wall in Case I at that time as initial conditions. The turbulent skin friction coefficients on the compliant and rigid walls in all cases have almost the same value of about 12.6 and the turbulent Reynolds number is about 137. No drag reduction is observed associated with the two compliant walls. Figure 10 shows that the log-law region is not shifted above the two compliant walls. The pertinent statistical quantities in Case I and Case II are compared with the reference case in figure 11. There is little difference between all cases for each of these statistical quantities. The compliant walls do not seem to statistically affect the turbulence in their vicinity and near the opposite rigid walls. But in the viscous region $y^+ < 10$, and only in this region, the maximum amplitude of streamwise vorticity is suppressed by the nearby compliant walls, see figure 12. The compliant walls do not seem to have a significant effect on

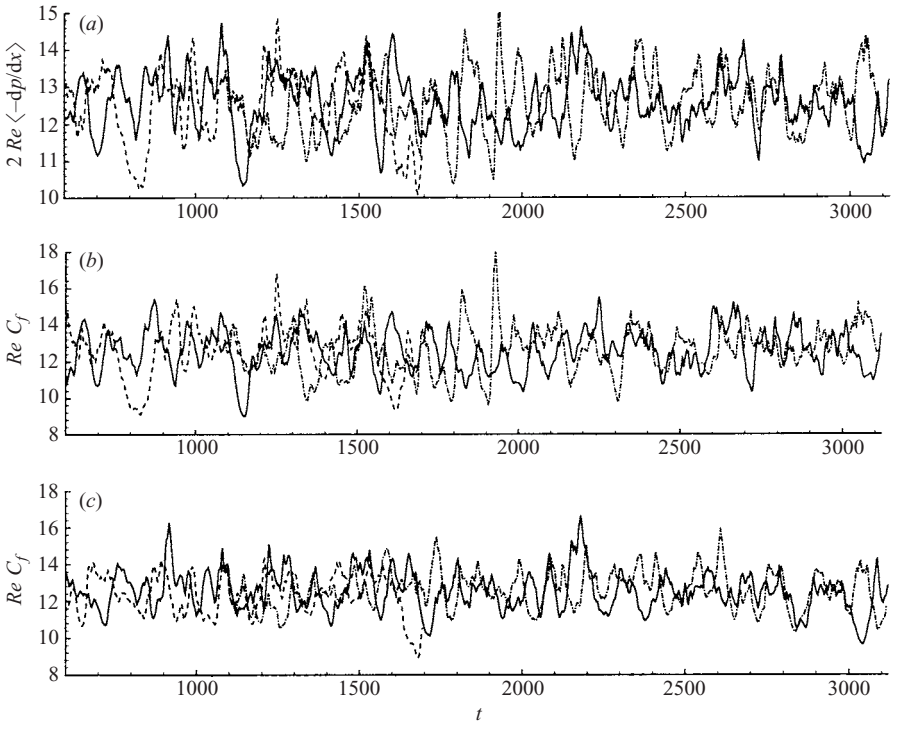

FIGURE 9. Time traces of (*a*) total drag, (*b*) skin friction on the compliant walls in Case I and Case II and on a rigid wall in the reference case and (*c*) skin friction on the rigid walls in Case I and Case II and on the other rigid wall in the reference case. Solid line: the rigid channel, dashed line: Case I, dash-dotted line: Case II.

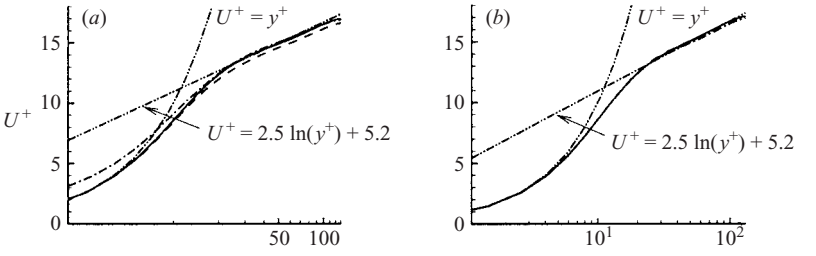

FIGURE 10. Mean streamwise velocity in all cases near (*a*) $y = -1$ (the average position of the complaint walls in Case I and Case II) and (*b*) $y = +1$. Solid line: the rigid channel, dashed line: Case I, dash-dotted line: Case II.

the statistics of the maximum amplitude of wall-normal vorticity, spanwise fluctuating vorticity or Reynolds shear stress.

The instantaneous compliant wall shape and the contours of wall-normal velocity on the compliant wall in Case I and Case II at two instants t_l and t_h are shown in figure 13. The skin friction on a compliant wall is low at t_l ($t_l = 814$ in Case I, $t_l = 1894$ in Case II) and high at t_h ($t_h = 1334$ in Case I, $t_h = 1933$ in Case II), see figure 14. The contours of streamwise fluctuating velocity and pressure at the surfaces close to and approximately parallel to the compliant wall in each case are plotted at the same two instants in figure 15 and figure 16. It can be seen that at the instants of low skin

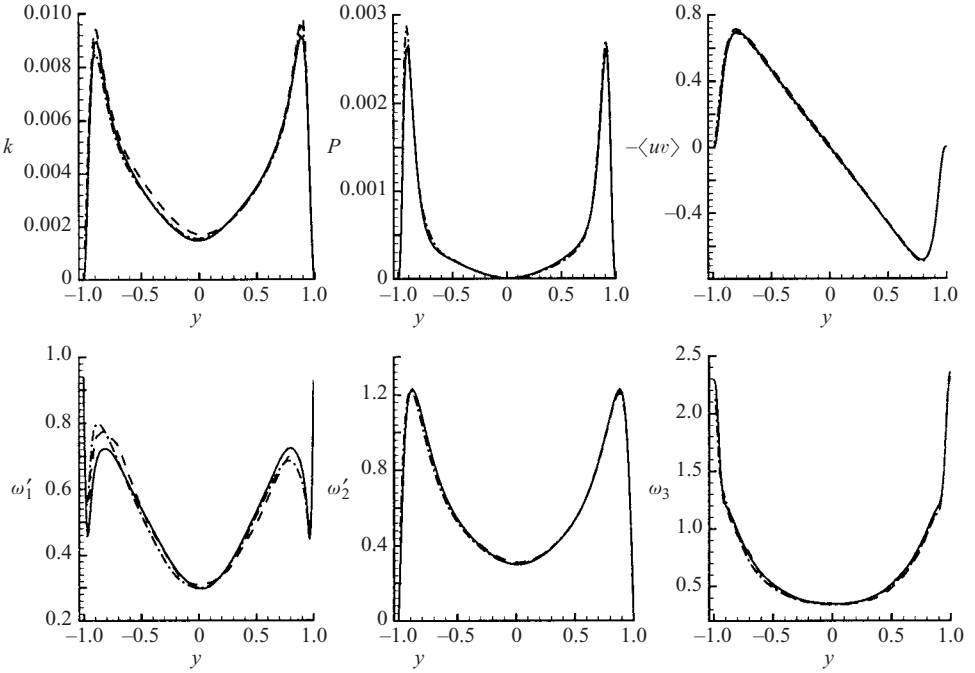

FIGURE 11. Comparison of turbulent kinetic energy k, turbulent kinetic energy production P, Reynolds shear stress $-\langle uv \rangle$, RMS streamwise vorticity ω_1', RMS wall-normal vorticity ω_2' and RMS spanwise fluctuating vorticity ω_3'. The average position of the compliant walls is at $y = -1$. Solid line: the reference case, dashed line: Case I, dash-dotted line: Case II.

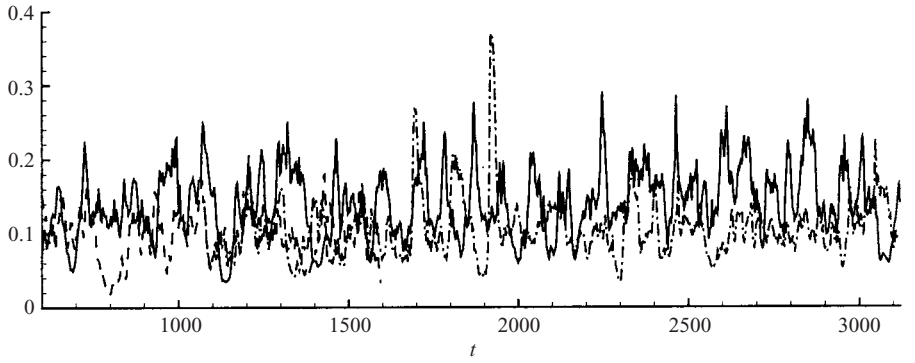

FIGURE 12. Time traces of maximum amplitude of streamwise vorticity in the region $y^+ < 10$ near the compliant walls in Case I and Case II and near a rigid wall in the reference case. Solid line: the reference case, dashed line: Case I, dash-dotted line: Case II.

friction at the compliant walls, the near-wall streaky structures are very obvious on these surfaces and pressure on them is out of phase with the wall-normal velocity on the corresponding compliant walls. The compliant walls form longitudinal ridges beneath low-speed streaks and corresponding grooves beneath high-speed streaks, even though the contours of the instantaneous wall-normal velocity at the walls are intermittent and oval-shaped. As shown in figure 17, the flows near the compliant walls are quiescent when the skin friction at the walls is low, while there are strong

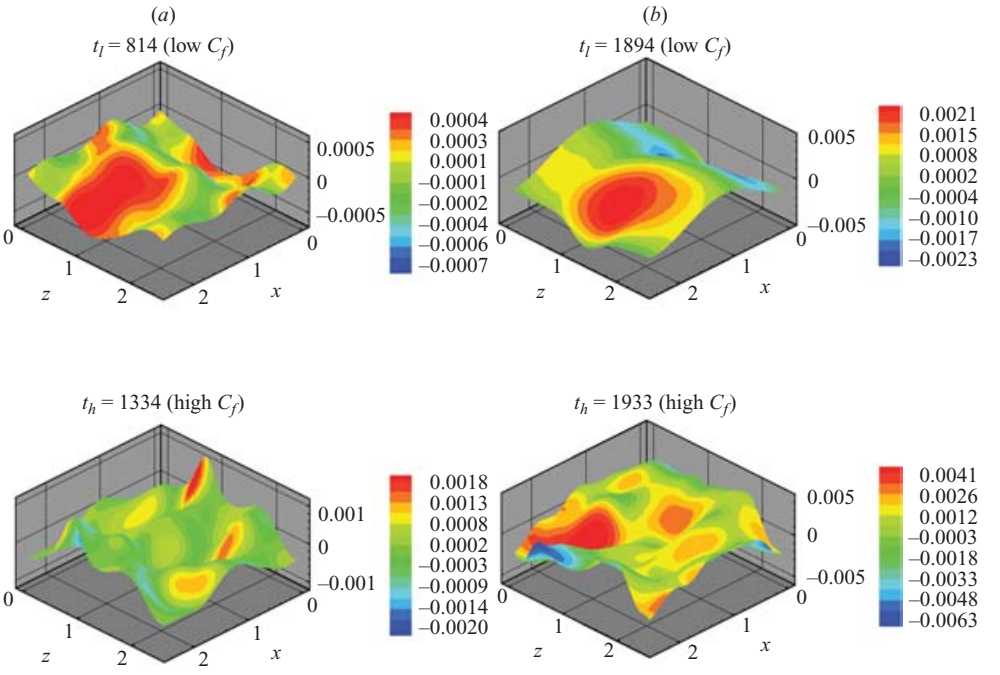

FIGURE 13. Displacement and contour of wall-normal velocity of the compliant walls in (*a*) Case I and (*b*) Case II, at the two instants shown in figure 14.

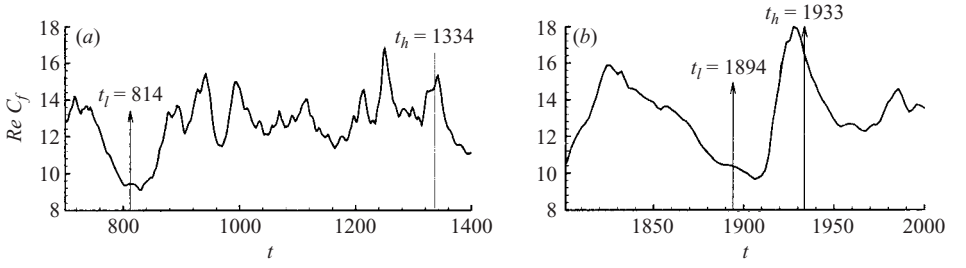

FIGURE 14. The time instants picked for output in (*a*) Case I and (*b*) Case II.

ejection and sweep events associated with vortices that are present in low-pressure regions when the skin friction at the walls is high. Correspondingly, the streamwise vorticity is of small amplitude near the compliant walls at the instants of low skin friction and large at instants of high skin friction, see figure 18.

Figure 19 shows the time history of the correlations between the velocity of the compliant wall and various quantities of the turbulence near the wall for the duration of low-drag and high-drag phases in Case I and Case II. It seems that these correlations do not directly reflect the fluctuating drag behaviour. The time-averaged values of these correlations and those between wall pressure and near-wall velocity at $y^+ = 3$ and $y^+ = 10$ for all the rigid and compliant walls are listed in table 2 for both cases. It can be seen that the correlations associated with the rigid walls for Case I and Case II are identical and are not affected by the substantially different mechanical properties of the compliant walls. Compared with the rigid walls, the compliant walls,

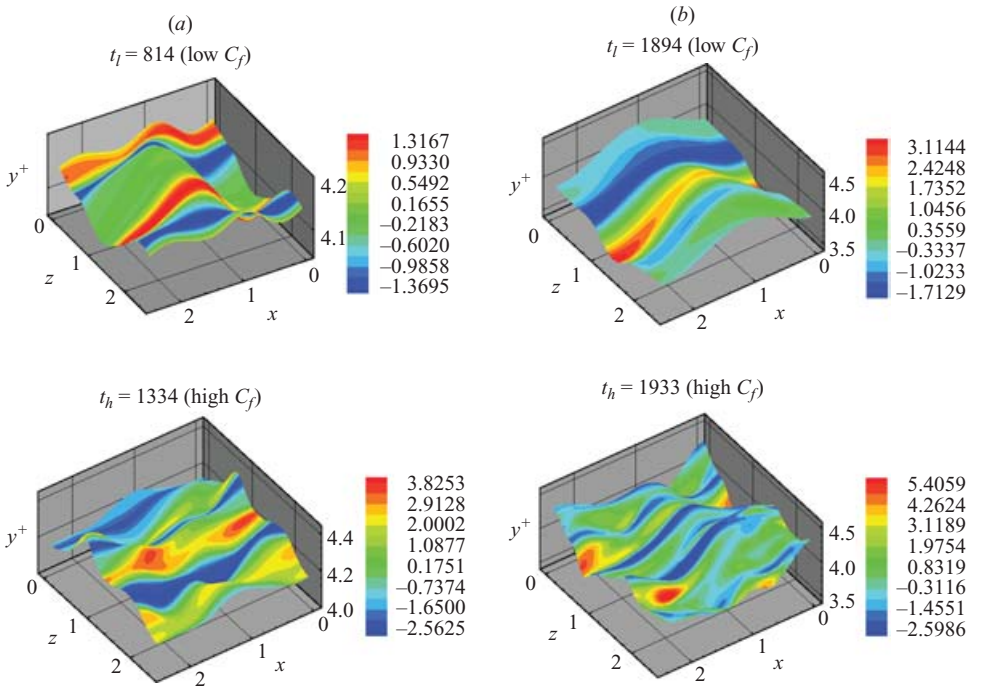

FIGURE 15. Contour of fluctuating streamwise velocity at surfaces approximately parallel to the compliant walls at the two instants in (*a*) Case I and (*b*) Case II.

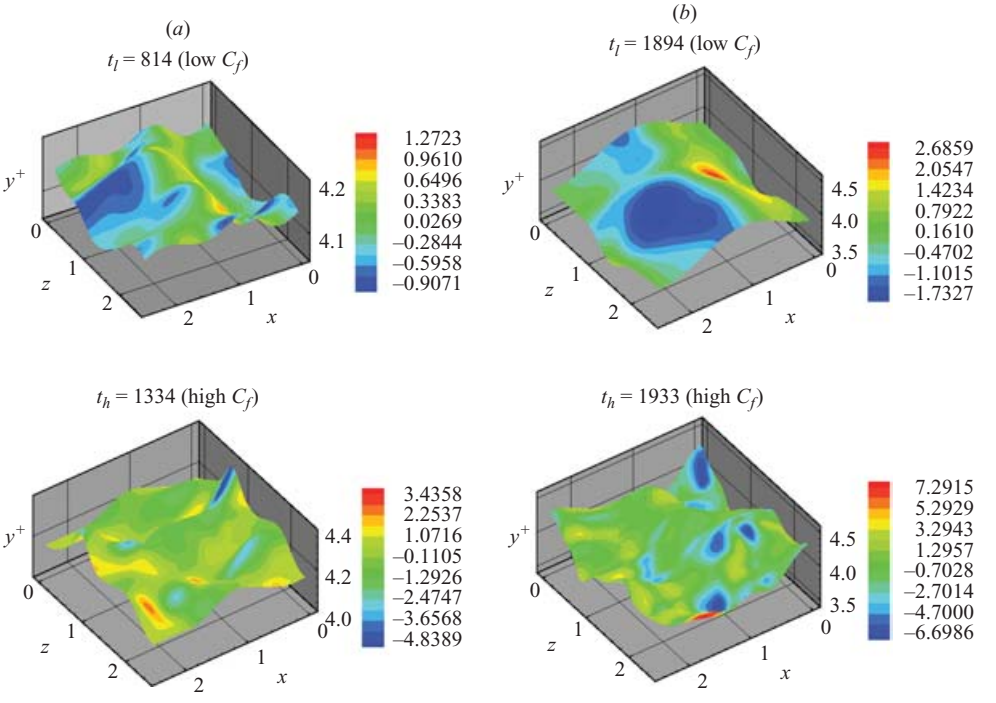

FIGURE 16. Contours of fluctuating pressure at the plane approximately parallel to the compliant walls at the two instants in (*a*) Case I and (*b*) Case II.

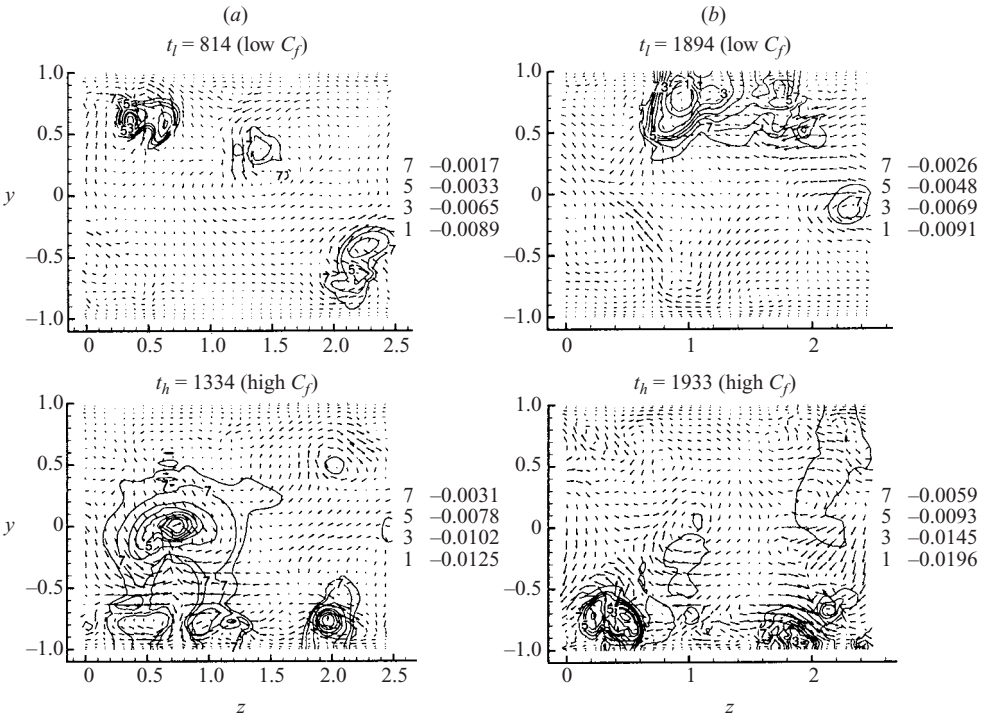

FIGURE 17. Contours of fluctuating pressure in the (z,y)-plane at distance $h/4$ from the channel inlet at the two instants in (*a*) Case I and (*b*) Case II.

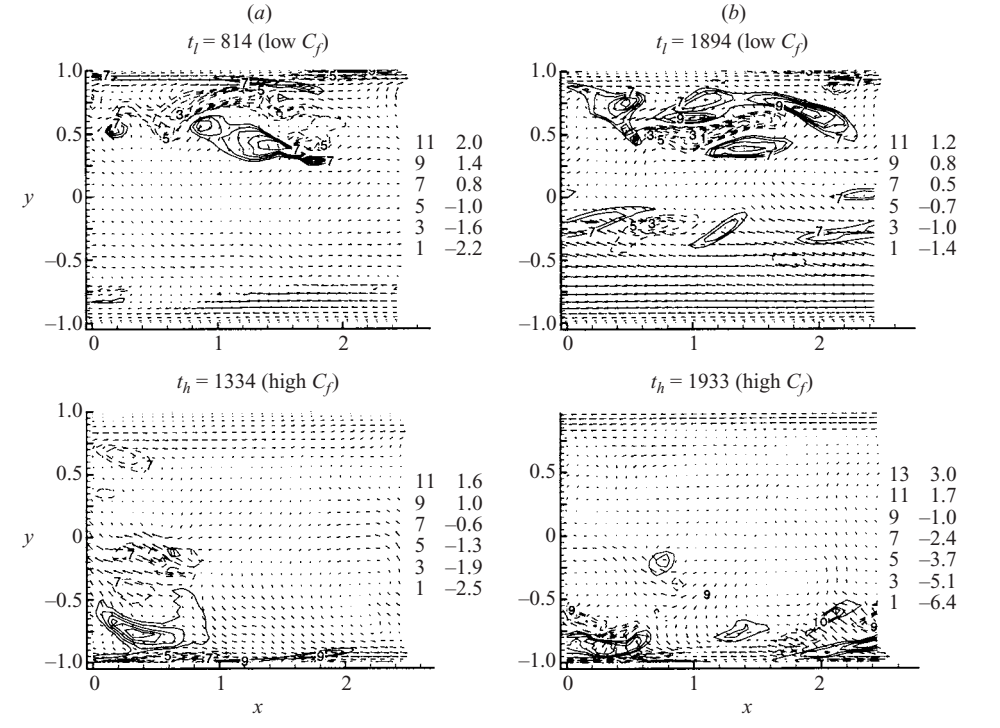

FIGURE 18. Contours of fluctuating streamwise vorticity in the (x,y)-plane one quarter period from the origin of the z-axis at the two instants in (*a*) Case I and (*b*) Case II.

	Case I		Case II	
Correlations	Rigid wall	Compliant wall	Rigid wall	Compliant wall
$\overline{\langle p_w v_1 \rangle}$	0.34	−0.49	0.34	−0.55
$\overline{\langle p_w v_2 \rangle}$	0.25	−0.27	0.25	−0.32
$\overline{\langle v_w p_w \rangle}$		−0.79		−0.80
$\overline{\langle v_w v_1 \rangle}$		0.20		0.47
$\overline{\langle v_w v_2 \rangle}$		−0.01		0.20

TABLE 2. Time-averaged values of correlations. The overbar denotes time average. p_w and v_w are the wall pressure and wall velocity respectively. v_1 and v_2 are the wall-normal velocity at $y^+ = 3$ and $y^+ = 10$ respectively.

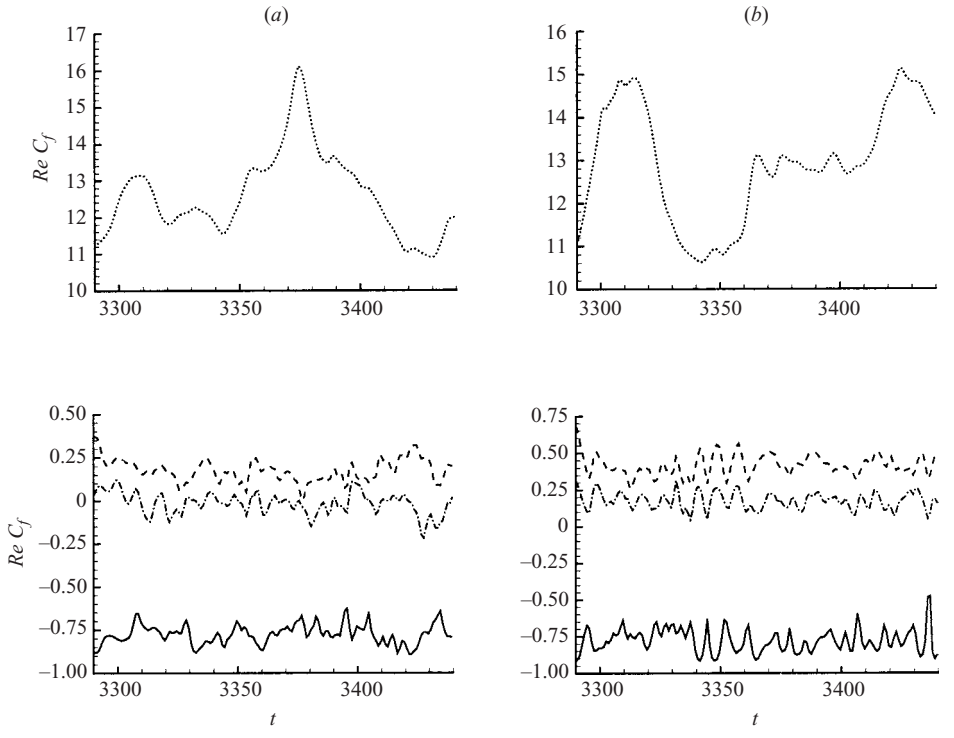

FIGURE 19. Time history of correlations between quantities of the compliant walls and near-wall turbulence for the duration of low-drag and high-drag phases in (*a*) Case I and (*b*) Case II. Dotted line: drag, solid line: $\langle v_w p_w \rangle$ (v_w and p_w are the wall velocity and wall pressure respectively), Dashed line: $\langle v_w v_1 \rangle$ (v_1 is the wall-normal velocity at $y^+ = 3$), Dash-dotted line: $\langle v_w v_2 \rangle$ (v_2 is the wall-normal velocity at $y^+ = 10$).

especially the softer wall of Case II show enhanced correlations between their driving wall pressure and the near-wall velocity at $y^+ = 3$ or $y^+ = 10$. The velocity and wall pressure on the compliant walls are correlated well negatively, which means the motion of the compliant walls follows the wall pressure very well. We will return to this observation below.

It is commonly assumed that a compliant wall may modify the near-wall coherent structures and their coherent motions. The near-wall quasi-streamwise vortices are regarded as playing a dominant role in near-wall turbulence production and transport (Robinson 1991). By applying blowing or suction on a channel wall with a rate exactly opposite to the normal component of the velocity at a prescribed y-position, say $y^+ = 10$, significant drag reduction has been achieved by Choi, Moin & Kim (1994) and the drag reduction mechanism has been related to the suppression of a source of new quasi-streamwise vortices above the wall. The pressure is, in general, high underneath the downwash region of two counter-rotating quasi-streamwise vortices and low underneath the upwash region of such vortices, as supported by figure 19 and table 2. Can we combine the idea of active turbulence control and the observations above to conceptually design a compliant wall for drag reduction? If the wall-normal velocity at a compliant wall is in phase with the pressure but out of phase with the near-wall velocity, and if it is intensive enough, it may suppress the formation of the quasi-streamwise vortices and result in drag reduction.

In order to investigate this idea, we decompose the wall pressure field into eddies, which may be represented by individual Fourier modes. Each eddy is associated with a time scale which can be estimated from the scale relation between length and time (Tennekes & Lumley 1972) or from the time corresponding to the peak in the time spectrum of the eddy energy. In eddy space, the compliant wall is a spring–damper system driven by a pressure eddy with a particular frequency. We thus need to choose the values of the wall parameters, which, of course, are functions of eddy size, so that the velocity of the compliant wall is in phase with the pressure. In order to find such values, we can study the transfer function $G(s)$, which is defined as the ratio of the Laplace transforms of the output signal ($\mathrm{d}\hat{\eta}/\mathrm{d}t$ in our case) and the input signal ($\hat{p}$) with zero initial conditions. Thus the amplitude and phase of the complex transfer function $G(s) = s\hat{\eta}(s)/\hat{p}_w(s)$ give the steady-state amplitude ratio and phase lag between the input and the output signals, commonly plotted in the so-called 'Bode diagram'. Figure 20 shows a Bode diagram for the system taking the pressure as input and the wall velocity as output. We can see that the phase lag between the wall velocity and the wall pressure ranges from $\pi/2$ to $3\pi/2$ as the frequency σ of the wall pressure changes. What this tells us is that it is impossible to obtain the desired positive correlation between the velocity and the pressure.

Thus, it appears that our idea of designing a compliant wall with elastic properties chosen in such a way that the dynamics of the wall would mimic the motion of the 'active wall' simulated by Kang & Choi (2000) may not work: according to our results above it is not possible, for any choice of parameters for the kind of compliant wall we were studying, to achieve the desired phase relation between the motion of the wall and near-wall velocities at about $y^+ = 10$. We should keep in mind, however, that the setup of our numerical experiments does not exhaust the potential configurations of a compliant wall. For example, if we had used a finite compliant panel similar to the ones described by Carpenter *et al.* (2000), then there is the possibility of wave reflection on the boundaries of the panel, which could change the situation significantly. We will come back to this point in our discussion below.

Bushnell *et al.* (1977) hypothesized that a successful compliant wall would delay the burst formation by producing a modulated pressure gradient superimposed upon the adverse gradient signal which normally triggers the bursts and suggested that as a minimum, the wall frequency required is probably of the order of 50 times the fundamental burst frequency. It has also been hypothesized that any variation in

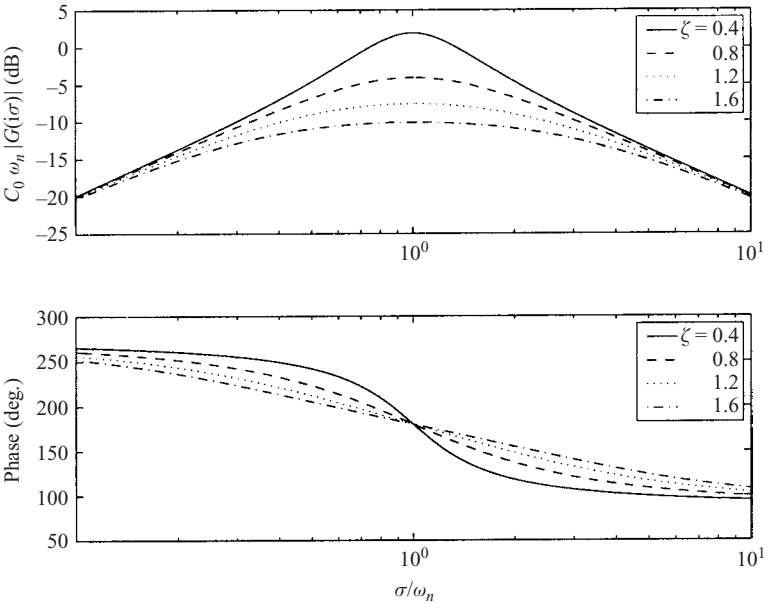

FIGURE 20. Bode diagram for the compliant wall system. $G(s)$ is the transfer function. σ, ω_n and ζ are defined in § 3.2.

the magnitude of dimensionless spanwise wall-streak spacing is accompanied by a change in the skin friction drag. The flow-visualization experiments by Lee, Fisher & Schwarz (1993) indicated low-speed wall streaks with increased spanwise spacing and elongated spatial coherence in a turbulent boundary layer over a single-layer viscoelastic compliant surface compared with those on a rigid surface. On the other hand, Gad-el-Hak *et al.* (1984) reported that no significant differences were found in the number of recorded streaks and the skin friction coefficients for turbulent boundary layers over PVC plastisol-gel compliant walls. In our simulations, the burst frequencies are about the same near all the compliant and rigid walls, see figure 9. The location, shape and spacing of streaky structures change with time and it is thus necessary to look at their long-time behaviour to obtain an accurate relationship between the average drag and their statistics. We did not observe significant modifications to the shape of the coherent structures in our simulations. The qualitative picture of turbulence over the compliant walls is about the same as over the rigid walls in a time sequence covering at least a burst period. Figure 21 shows the spanwise auto-correlation function for streamwise fluctuating velocity u in Case I, Case II and the reference case. Little quantitative difference is observed near $y = -1$, which may indicate that the spanwise coherence of streaky structures does not change.

It is interesting to note that we could cause a reduction in skin-friction drag by up to 12%, accompanied by a corresponding upward shift of the log-law region and reduction in the magnitude of the pertinent statistical quantities of the turbulence near the compliant wall, by unphysically driving a soft compliant wall with the negative pressure signal. We found that such an 'anti-compliant wall' forms a longitudinal ridge beneath a high-speed streak and a corresponding groove beneath a low-speed streak when near-wall streaky structures are not broken down. Kang & Choi (2000) made similar observations for their active wall control for skin friction

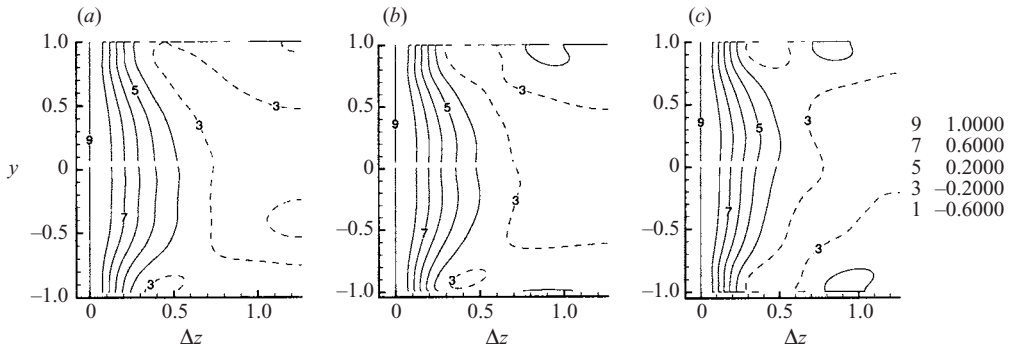

FIGURE 21. Contours of spanwise auto-correlation function for streamwise fluctuating velocity u in (a) Case I, (b) Case II and (c) the reference case.

reduction. However, if the right pressure (with the correct sign) is acting on such a compliant wall, the wall–fluid interaction becomes unstable. For stiffer compliant walls, with parameters similar to our Cases I and II, however, artificially inverting the sign of the pressure disturbances has no statistically significant effect on average drag.

4. Discussion

In our numerical simulations we have observed that the convergence to a steady-state average value of the turbulent skin friction drag on a compliant wall takes as long as up to $O(Re)$ eddy turn-over times. First results of our direct numerical simulation of the turbulence on the compliant walls indicate no drag reduction over such long time periods. We note that Endo & Himeno (2002) have reported a drag reduction of 7% in their numerical simulation of turbulent flow over a compliant surface. However, their averaging times were much shorter than ours. The simulation data they used to calculate their statistics spanned 700 viscous times, which corresponds to about 100 eddy turn-over times. We have found that we can obtain an apparent drag reduction that is similar to the one found by Endo & Himeno if we average over an appropriately chosen interval that is as short as theirs. Unfortunately, in our simulations, any such 'drag reduction' all but disappears after extending our averaging interval to the times reported here.

If we assume that for successful drag reduction the wall should move in a similar fashion to the one used in the study by Kang & Choi (2000) , meaning that there should be a positive correlation between the wall velocity and the fluctuating pressure at the wall, then our evidence seems to indicate that the particular design of a compliant wall we have investigated may not be promising. We note, however, that these findings do not yet rule out successful drag reduction using other approaches. One option would be to allow for non-uniform elasticity properties of the wall, with a stiffness that varies over the compliant surface. Another potentially promising avenue would be to follow the lead of Carpenter *et al.* (2000) and replace our infinite compliant wall with finite compliant panels of an appropriate (and yet to be determined) size. In that case one could use fixed boundary conditions at the ends of the panels, which would cause reflection of the elastic waves in the panel. Such wave reflections might allow us to achieve the phase relations we need for positive drag reduction. We will study this idea in further work.

While our current results are preliminary in nature, they do provide input data for a proper orthogonal decomposition (POD) analysis and low-dimensional dynamical systems models based on POD eigenfunctions, see Rempter *et al.* (2001). Such models can provide insight into the mechanisms of the interaction between turbulence and a compliant wall from a dynamical-systems perspective, and can help us choose compliant walls for drag minimization by adjusting the model parameters even though the POD analysis is based on direct simulation data that do not exhibit any drag reduction.

To conserve resources, we performed the simulations in a minimal flow unit. The use of periodic boundary conditions can be expected to distort the flow physics when the size of the periodic box is too small. It is not clear in how far (or whether at all) the results for the minimal channel can be extrapolated to the full channel. According to Yeo, Zhao & Khoo (2001), compliant surfaces with low damping are susceptible to convective instability, which gives way to an absolute instability when the surfaces become highly damped. The compliant walls we used have very high damping while the Reynolds number of the simulated turbulent flow is low, so we may assume that all critical wall modes can be represented in our domain size if there are no static-divergence waves.

Supposing we are looking at a turbulent flow in an infinite compliant channel, can we just cut out a large enough rectangular compliant channel and apply periodic boundary conditions to simulate the flow? We probably can if any spatial auto-correlations across the length and width of the channel decay to zero, the interaction between the flow and the compliant wall is stable, and the waves excited at a point of the compliant wall die away before they reach the edge of the region. The last condition can be checked by analysing the compliant wall dynamics. Let us consider an infinite compliant wall under the action of pressure disturbances $p(x,t)$, i.e. uniform in the z-direction. A mathematical model for the compliant wall motion can then be given as

$$\left.\begin{aligned} &C_0\frac{\partial^2\eta}{\partial t^2}+C_1\frac{\partial\eta}{\partial t}+C_2\frac{\partial^4\eta}{\partial x^4}+C_3\eta-C_x\frac{\partial^2\eta}{\partial x^2}=-p(x,t),\ -\infty<x<+\infty, t>0,\\ &\eta(x,0)=\phi(x),\quad \frac{\mathrm{d}\eta(x,0)}{\mathrm{d}t}=\psi(x). \end{aligned}\right\} \tag{4.1}$$

When C_2 is very small and is neglected, we can choose $C_1=2\sqrt{C_0C_3}$ such that the analytical solution to $\eta(x,t)$ can be found as

$$\begin{aligned}\eta(x,t)=&\frac{1}{2}\exp\left(-\frac{C_1t}{2C_0}\right)\left[\phi(x-at)+\phi(x+at)+\frac{1}{a}\int_{x-at}^{x+at}\psi(\xi)\,\mathrm{d}\xi\right]\\ &-\frac{1}{2aC_0}\int_0^t\left\{\exp\left[-\frac{C_1(t-\tau)}{2C_0}\right]\int_{x-a(t-\tau)}^{x+a(t-\tau)}p(\xi,\tau)\,\mathrm{d}\xi\right\}\mathrm{d}\tau,\end{aligned} \tag{4.2}$$

where $a=\sqrt{C_x/C_0}$ is the wave speed. The amplitude of a wave excited at one point on the compliant wall will be damped to $100\exp(LC_1/2aC_0)\%$ of its initial value after it propagates a distance of L. For Case I and Case II of our simulations, this percentage is respectively about 0.022% and 0% for $L=L_1$. If small C_2 is not neglected and $C_1>2\sqrt{C_0C_3}$, from the dispersion relation and pressure spectra on the wall we know that shorter waves can survive for a longer distance due to their faster speed, but they are of very small initial amplitude. If both C_2 and C_x are set to be zero, the

compliant wall becomes a spring–damper system and does not support wave-like solutions.

This project is supported by Air Force under contract AFOSR F49620-96-1-0329.

REFERENCES

Bridges, T. L. & Morris, P. J. 1984 Differential eigenvalue problems in which the parameter appears nonlinearly. *J. Comput. Phys.* **55**, 437–460.

Bushnell, D. M., Hefner, J. N. & Ash, R. L. 1977 Effect of compliant wall motion on turbulent boundary layers. *Phys. Fluids* A **20**, S31.

Carlson, H. A., Berkooz, G. & Lumley, J. L. 1995 Direct numerical simulation of flow in a channel with complex, time-dependent wall geometries: a pseudospectral method. *J. Comput. Phys.* **121**, 155–175.

Carpenter, P. W., Davies, C. & Lucey, A. D. 2000 Hydrodynamics and compliant walls: Does the dolphin have a secret? *Current Science* **79**, 758–765.

Carpenter, P. W. & Morris, P. J 1990 The effect of anisotropic wall compliance on boundary-layer stability and transition. *J. Fluid Mech.* **218**, 171–223.

Choi, H., Moin, P. & Kim, J. 1994 Active turbulence control for drag reduction in wall-bounded flows. *J. Fluid Mech.* **262**, 75–110.

Davies, C. & Carpenter, P. W. 1997 Numerical simulations of the evolution of Tollmien–Schlichting waves over finite compliant panels. *J. Fluid Mech.* **335**, 361–392.

Endo, T. & Himeno, R. 2002 Direct numerical simulation of turbulent flow over a compliant surface. *J. Turbulence* **3**, 1–10.

Gad-el-Hak, M. 1986 Boundary layer interactions with compliant coatings: an overview. *Appl. Mech. Rev.* **3**, 511–524.

Gad-el-Hak, M. 1998 Compliant coatings: The simpler alternative. *Expl Therm. Fluid Sci.* **16**, 141–156.

Gad-el-Hak, M., Blackwelder, R. F. & Riley, J. J. 1984 On the interaction of compliant coats with boundary-layer flows. *J. Fluid Mech.* **140**, 257–280.

Gajjar, J. S. B. & Sibanda, P. 1996 The hydrodynamic stability of channel flow with compliant boundaries. *Theoret. Comput. Fluid Dyn.* **8**, 105–129.

Jiménez, J. & Moin, P. 1991 The minimal flow unit in near-wall turbulence. *J. Fluid Mech.* **225**, 213–240.

Kang, S. & Choi, H. 2000 Active wall motions for skin-friction drag reduction. *Phys. Fluids* **12**, 3301–3304.

Kireiko, G. V. 1991 Interaction of wall turbulence with a compliant surface. *Fluid Dyn.* **25**, 550.

Kramer, M. O. 1961 The Dolphin's Secret. *J. Am. Soc. Nav. Engrs.* **73**, 103–107.

Larose, P. G. & Grotberg, J. B. 1996 Flutter and long-wave instabilities in compliant channels conveying developing flows. *J. Fluid Mech.* **331**, 37–58.

Lee, T., Fisher, M. & Schwarz, W. H. 1993 Investigation of the stable interaction of a passive compliant surface with a turbulent boundary layer. *J. Fluid Mech.* **257**, 373–401.

Lucey, A. D., Cafolla, G. J., Carpenter, P. W. & Yang, M. 1997 The nonlinear hydroelastic behaviour of flexible walls *J. Fluids Struct.* **11**, 717–744.

Lucey, A. D. & Carpenter, P. W. 1995 Boundary layer instability over compliant walls: comparison between theory and experiment. *Phys. Fluids* **7**, 2355–2363.

Lumley, J. L. & Blossey, P. N. 1998 Control of turbulence. *Annu. Rev. Fluid Mech.* **30**, 311–327.

Rempfer, D., Blossey, P., Parsons, L. & Lumley, J. L. 2001 Low-dimensional dynamical model of a turbulent boundary layer over a compliant surface: preliminary results. In *Fluid Dynamics and the Environment: Dynamical Approaches* (ed. J. Lumley). Springer.

Reutov, V. P. & Rybushkina, G. V. 1998 Hydroelastic instability threshold in a turbulent boundary layer over a compliant coating. *Phys. Fluids* **10**, 417–425.

Riley, J. J., Gad-el-Hak, M. & Metcalfe, R. W. 1988 Compliant coatings. *Annu. Rev. Fluid Mech.* **20**, 393–420.

Robinson, S. K. 1991 Coherent motions in the turbulent boundary layer. *Annu. Rev. Fluid Mech.* **23**, 601–639.

Semenov, B. N. 1991 On conditions of modelling and choice of viscoelastic coatings for drag reduction. In *Recent Developments in Turbulence Management* (ed. K.-S. Choi), pp. 241–262. Kluwer.

Tennekes, H. & Lumley, J. L. 1972 Spectral dynamics. In *A First Course in Turbulence*, pp. 248–287. MIT Press.

Yeo, K. S., Khoo, B. C. & Zhao, H. Z. 1999 The convective and absolute instability of fluid flow over viscoelastic compliant layers. *J. Sound Vib.* **223**, 379–398.

Yeo, K. S., Zhao, H. Z. & Khoo, B. C. 2001 Turbulent boundary layer over a compliant surface: absolute and convective instabilities. *J. Fluid Mech.* **449**, 141–168.

Zebib, A. 1984 A Chebyshev method for the solution of boundary value problems. *J. Comput. Phys.* **53**, 443–455.